Journal of Alloys and Compounds 509 (2011) 3553–3558

Contents lists available at ScienceDirect

Journal of Alloys and Compounds

journal homepage: www.elsevier.com/locate/jallcom

Eu^{2+}/Sm^{3+} ions co-doped white light luminescence $SrSiO_3$ glass-ceramics phosphor for White LED

Zhiguang Cui, Renguang Ye, Degang Deng, Youjie Hua, Shilong Zhao, Guohua Jia, Chenxia Li, Shiqing Xu *

College of Materials Science and Engineering, China Jiliang University, Hangzhou 310018, China

ARTICLE INFO

Article history:
Received 10 September 2010
Received in revised form 8 December 2010
Accepted 8 December 2010
Available online 15 December 2010

Keywords:
Glass ceramics
Eu^{2+}/Sm^{3+} co-doped
$SrSiO_3$ nano-crystals
Optical properties
White LED

ABSTRACT

Eu^{2+}/Sm^{3+} co-doped silicate glass was prepared by high temperature melting under reducing atmosphere and the Eu^{2+}/Sm^{3+} co-doped $SrSiO_3$ transparent glass-ceramics were obtained after heat-treatment. X-ray diffraction (XRD) and Raman spectra confirmed the formation of $SrSiO_3$ nano-crystals in the glass matrix. The photoluminescence excitation (PLE) spectra and photoluminescence (PL) spectra of the samples were measured. A broad emission band from 400 nm to 550 nm due to the $4f^6 5d^1 \rightarrow 4f^7$ transitions of Eu^{2+} was observed, as well as several sharp emission peaks at 563 nm, 600 nm, 646 nm and 713 nm ascribed to the $4f \rightarrow 4f$ transitions of Sm^{3+}. The luminescence properties of the glass ceramics with different molar ratio of Eu^{2+}/Sm^{3+} were studied and the corresponding chromaticity coordinates were calculated. The ultraviolet light-emitting diode (UV-LED) excitable glass-ceramics emitting white light were obtained by tuning the relative emission intensity of Eu^{2+} and Sm^{3+}. The results indicate that the Eu^{2+}/Sm^{3+} co-doped $SrSiO_3$ transparent glass-ceramics can be used as a potential matrix material for White LED under UV-LED excitation.

1. Introduction

White light-emitting diodes (LEDs) have been considered as a potential replacement for the conventional illumination devices in the viewpoints of low electric consumption, high brightness, long lifetime and environment friendly characters [1–3]. One of the methods for making white LED is the combination of an ultraviolet (UV) or near-ultraviolet (NUV) LED chip with tricolor phosphors (red, green and blue) packed with organic resins. Compared with white LED using blue LED chip and the YAG:Ce^{3+} phosphor, it has high color rendering and is believed to offer the greatest potential for high efficiency solid state lighting [4]. Because of the remarkable progress in the development of LED chips with emission at 300–420 nm, more and more attention has been paid to the development of new phosphors converting white LED that can be excited efficiently in this band [5–10].

In general, the phosphors converting white LED are embedded in organic resins. However, there are several problems in this type of white LED, including the large difference of refractive index between phosphors and organic resins which will lead to high amount of scattering light, and the poor heat-resistance which will lead to the degradation of luminous intensity and the change of emission color [11]. Therefore, the glass-ceramics phosphors have been studied as a promising material due to its better heat-resistance than organic resins, available facility of production process, easy of formability, and low porosity compared with sintered ceramics [12–18].

Additionally, Eu^{2+} activated phosphors are suitable for the tricolor phosphor converting white LED, because excited by UV or NUV they show broad emission band due to the $4f^6 5d^1 \rightarrow 4f^7$ transitions of Eu^{2+} coupled to the host lattice [19–22]. The emission color of Eu^{2+} in oxide hosts is usually ranging from violet to yellow, while Sm^{3+} doped phosphors show orange or red emission by $4f \rightarrow 4f$ transitions, which can improve color rendering of the Eu^{2+} activated phosphors by compensating the absence of red wavelength region. Though the Sm ions can take a divalent state, depending on the host composition and the preparation condition, the tendency of reduction is much smaller than that of Eu ions [13,23]. Therefore, it is possible to prepare Eu^{2+}/Sm^{3+} co-doped glass and glass-ceramics by choosing an appropriate reduction condition, which may exhibit an excellent color rending index (CRI). The luminescence properties of Eu^{2+} activated strontium metalsilicates ($SrSiO_3$) powder phosphors have been reported by some workers [24,25]. In this letter, we reported the preparation and spectral analysis of the UV-LED excitable white light emitting Eu^{2+}/Sm^{3+} co-doped glass ceramics phosphors containing $SrSiO_3$ nano-crystals.

2. Experimental

The glass composition comprised $60SiO_2$–$40SrO$–$0.01Eu_2O_3$–xSm_2O_3 (in mol%, $x = 0.02, 0.04, 0.06, 0.08, 0.1$). The raw materials are reagent grade SiO_2, $SrCO_3$, Eu_2O_3

* Corresponding author. Tel.: +86 571 86835781; fax: +86 571 28889527.
E-mail address: sxucjlu@hotmail.com (S. Xu).

0925-8388/$ – see front matter © 2010 Elsevier B.V. All rights reserved.
doi:10.1016/j.jallcom.2010.12.058

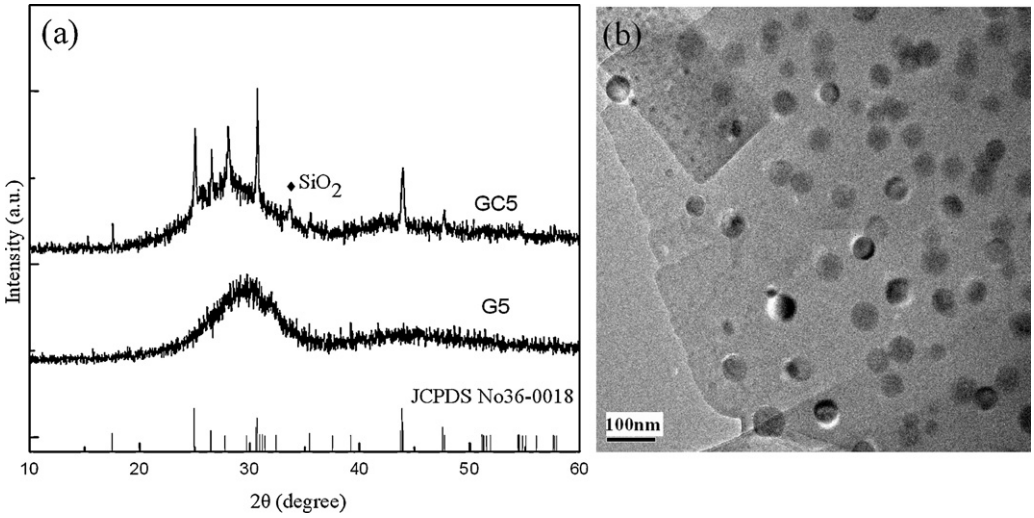

Fig. 1. (a) XRD patterns of G5 and GC5 and (b) TEM micrograph of GC5.

and Sm_2O_3. The materials were fully mixed in an agate mortar. An alumina crucible containing the mixed materials was placed in another lager alumina crucible which was filled with graphite to enhance the reducing effect. They were melted at 1560 °C for 1 h under the reducing atmosphere with 95%N_2–5%H_2. The melts were poured onto a preheated steel plate and cooled down to room temperature. The glasses were cut into 5 mm × 5 mm × 2 mm size and named as G1 (x = 0.02), G2 (x = 0.04), G3 (x = 0.06), G4 (x = 0.08) and G5 (x = 0.1), respectively. Thermal properties were measured by differential thermal analysis (DTA) at rate of 10 °C/min. The results showed that the transition temperature was 780 °C and crystallization peak temperature was 1030 °C. So G1, G2, G3, G4 and G5 were heat treated at 1030 °C for 2 h to obtain the glass ceramics, which were named as GC1, GC2, GC3, GC4 and GC5, respectively. The crystalline phases of the samples were identified by X-ray diffraction (XRD) measurement with a Cu-Ka radiation source. The fluorescence decay curves, photoluminescence (PL) and photoluminescence excitation (PLE) spectra of the glass and glass ceramics were measured by a Jobin-Yvon FL3-211-P spectrofluorometer equipped with a Xe flash lamp. The Raman spectra were recorded on a SL Raman spectrophotometer P1-532 HR within the range of 200–1400 cm^{-1}. All the measurements were carried out at room temperature.

3. Results and discussion

Fig. 1(a) presents the XRD patterns of the glass (G5) and glass-ceramics (GC5). The XRD pattern glass was completely amorphous with no diffraction peaks. After heat treatment, the XRD pattern of glass-ceramics showed intense diffraction peaks, which were well accordant with JCPDS card (NO. 36-0018) of the $SrSiO_3$ crystal except one small peak resulted by the impurities of SiO_2. From the XRD patterns, the mean size of $SrSiO_3$ nano-crystals, calculated by Scherrer equation, was about 30 nm. The TEM image of the sample GC5, shown in Fig. 1(b), demonstrated that nano-particles sized 25–35 nm was distributed homogenously among the glass matrix, which was consistent with the previous calculated result. Due to much smaller size of precipitated $SrSiO_3$ nano-crystals than wavelength of visible light, the Eu^{2+}/Sm^{3+} co-doped glass-ceramics remain transparent.

Fig. 2 shows the Raman spectra of the glass and glass-ceramics doped with 0.02 mol Eu^{2+} and 0.2 mol Sm^{3+} (G5 and GC5) at the range of 200–1400 cm^{-1}. In silicate glasses [26], the band at 550 cm^{-1} is assigned to bending vibration of Si–O–Si bonds, and at 880, 930, 970, 1030 and 1070 cm^{-1} are assigned to symmetric stretching vibration of SiO_4 tetrahedra with 4, 3, 2, 1 and 0 non-bridging oxygens, respectively. In the Raman spectrum of glass (G5), there were three obvious scattering peaks at 1055, 948, and 595 cm^{-1}, which moved to lower frequencies at 1052, 930, and 555 cm^{-1} peak in glass-ceramics (GC5). After heat treatment, the bands got structurized and new bands at 261, 284, 328, 395, 468, 495 and 641 cm^{-1} were found, and match the bending vibrations peaks of Si–O–Si bonds of $[SiO_3]^{2-}$ in $MgSiO_3$ [27,28], which also indicated that the $SrSiO_3$ nano-crystals were formed in Eu^{2+}/Sm^{3+} co-doped glass-ceramics. In addition, several weak intensity bands at 751, 968 and 1024 cm^{-1} were also observed, which could be ascribed to the vibrations of Si–O–Al bonds, symmetric stretching vibration of SiO_4 tetrahedra with 2 and 1 non-bridging oxygens, respectively. The Al ions might come from the alumina crucible.

The PLE and PL spectra of the 0.02 mol Eu^{2+} and 0.2 mol Sm^{3+} co-doped glass and glass-ceramics (G5 and GC5) are presented in Fig. 3. As shown in Fig. 3(a), the PLE spectra of GC5 were monitored at 505 nm and 600 nm respectively. The broad excitation band ranging from 300 nm to 450 nm could be attributed to the $4f^7 \rightarrow 4f^65d^1$ transitions of Eu^{2+} ions, while for Sm^{3+} several narrow bands centered at 345 nm, 362 nm, 376 nm, 407 nm, 418 nm and 438 nm were assigned to transitions of $^6H_{5/2} \rightarrow {}^3H_{7/2}$, $^6H_{5/2} \rightarrow {}^4L_{17/2}$, $^6H_{5/2} \rightarrow {}^4K_{13/2}$, $^6H_{5/2} \rightarrow {}^4F_{7/2}$, $^6H_{5/2} \rightarrow ({}^6P_{5/2}, {}^4P_{5/2})$, $^6H_{5/2} \rightarrow {}^4G_{9/2}$[29,30]. Apparently, the glass ceramics can be efficiently excited by several light in the UV region, and in this letter 365 nm was chosen as the excite light. In Fig. 3(b) a broad emission band from 400 nm to 550 nm due to the $4f^65d^1 \rightarrow 4f^7$ transitions of Eu^{2+} was observed, as well as several sharp emission peaks at 563 nm, 600 nm, 646 nm and 713 nm ascribed to

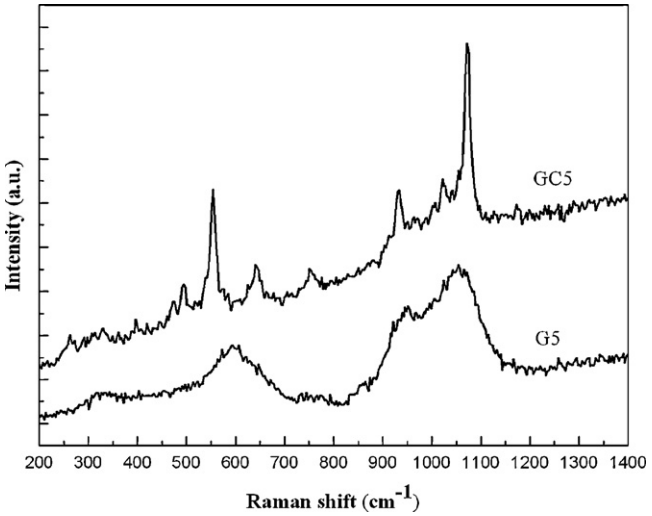

Fig. 2. Raman spectra of G5 and GC5 at the range of 200–1400 cm^{-1}.

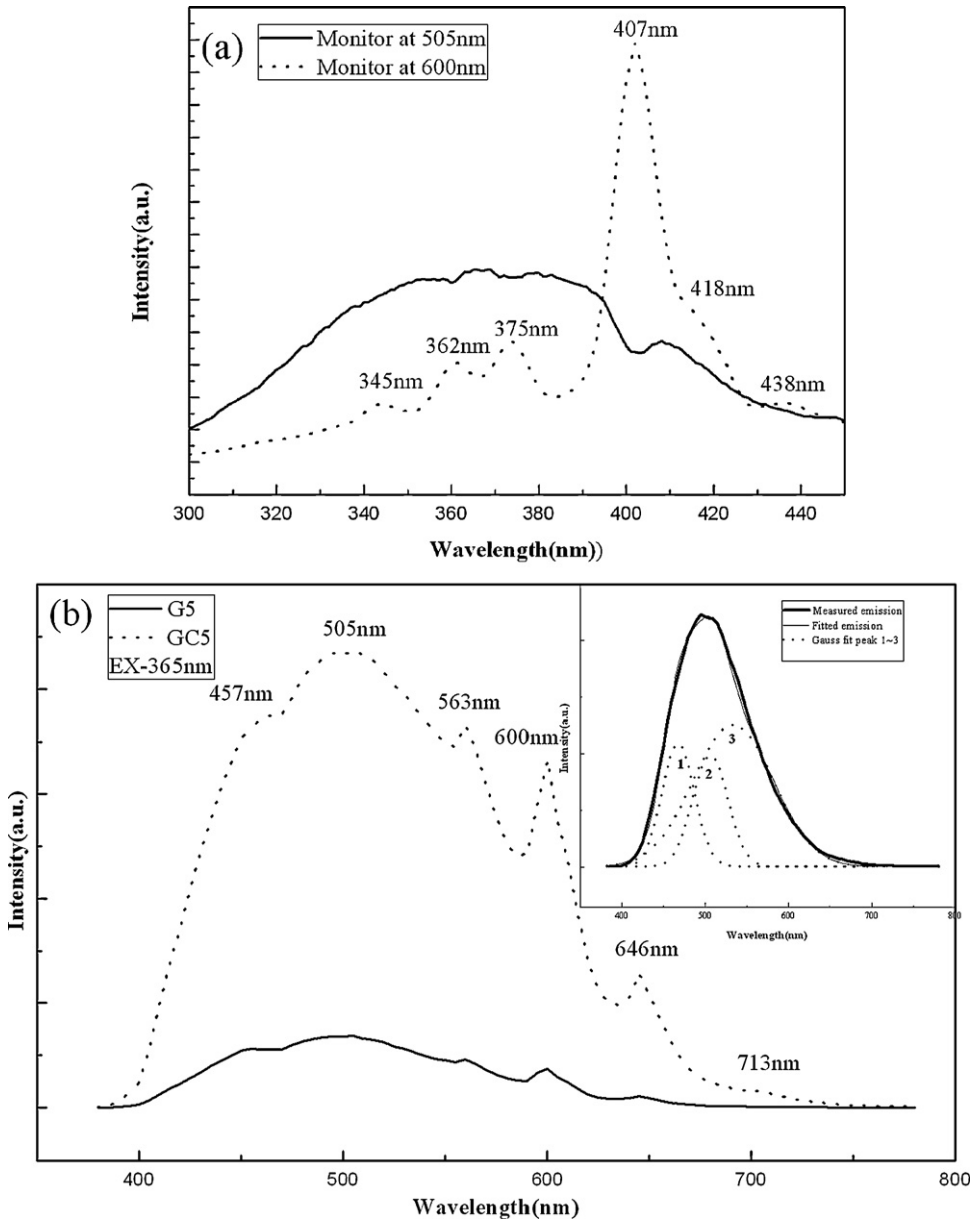

Fig. 3. The PLE and PL spectra of G5 and GC5: (a) PLE spectra of GC5 (monitored at 505 nm and 600 nm respectively); (b) PL spectra of G5 and GC5, the inset shows the Multi-peak fitting emission spectra of the Eu^{2+} single doped glass ceramics.

the $^4G_{5/2} \rightarrow {}^6H_{5/2}$, $^4G_{5/2} \rightarrow {}^6H_{7/2}$, $^4G_{5/2} \rightarrow {}^6H_{9/2}$ and $^4G_{5/2} \rightarrow {}^6H_{11/2}$ transitions of Sm^{3+}. The trivalent samarium has a fundamental level $^6H_{5/2}$ and three main emitting levels $^4G_{5/2}$, $^4F_{3/2}$ and $^4G_{7/2}$ located at 17860, 18857 and 20009 cm^{-1}, respectively, which give visible emissions (reddish-orange). Sm^{3+} also has a series of levels between 28573 and 17860 cm^{-1} very close to each other which allow non-radiative (NR) relaxation to the $^4G_{5/2}$ level. There were two emission bands of Eu^{2+} ions, centered at 457 nm and 505 nm respectively, which could be attributed to different Eu^{2+} ions substituted different Sr^{2+} sites in $SrSiO_3$ nano-crystals. Moreover, the 505 nm emission band is much broader than the 457 nm one, so using Gaussian fitting, the emission spectra of the Eu^{2+} single doped glass ceramics can be Multi-peak fitted into there Gaussians peaks with maxima at about 467 nm, 502 nm and 529 nm respectively on an energy scale, as can be seen in the inset picture in Fig. 3(b). Sr ions are all eight coordinate in $SrSiO_3$ nano-crystals, while there are three different kinds of strontium sites (Sr(1), Sr(2) and Sr(3) with average Sr–O distances of 2.68 Å, 2.65 Å and 2.60 Å, respectively). Eu^{2+} ions can substitute either site from the viewpoints of the ion radius and the charge valence [31–33]. Additionally, the Eu^{2+} ions are very sensitive to the around crystal field of the host. When the crystal environments are analogous, the Eu^{2+} with a shorter Eu^{2+}–O^{2-} distance will give a longer wavelength emission. So we ascribed the two longer wavelength emission at 502 nm and 529 nm to the emission of Eu^{2+} ions on Sr(1) and Sr(2) sites respectively. The much higher energy emission at 457 nm of Eu^{2+} on Sr(3) sites could be explained by means of preferential orientation of a d orbital of Eu^{2+} ions [34,35].

Compared with the glass, significant enhancement of the photoluminescence intensity was also observed, which could be ascribed to the precipitated lower phonon energy of $SrSiO_3$ nano-crystals in the glass-ceramics [36]. The intensity of photoluminescence was very sensitive to the multi-phonon relaxation rate of the rare-earth ions, which strongly depends on the phonon energy of their matrix. The lower the phonon energy of host was, the longer the lifetime and higher quantum efficiency of excited levels were, and con-

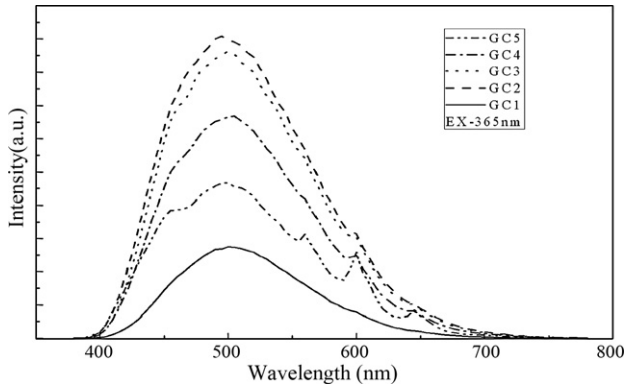

Fig. 4. PL spectra of GC1, GC2, GC3, GC4 and GC5 with λ_{ex} = 365 nm.

sequently the stronger the emission intensity was [37]. Based on the results of Raman analysis as shown in Fig. 2, bending vibration of Si–O–Si bonds (595 cm^{-1}) and the symmetric stretching vibrations of SiO_4 tetrahedra with 3 and 0 non-bridging oxygens (948 and 1055 cm^{-1}) in glass moved to lower energies at 555, 930, and 1052 cm^{-1} in glass-ceramics. It can be concluded that the maximum phonon energy of glass-ceramics decreased after heat treatment. At the same time, new lower energy stretching vibrations at 248, 284, 312, 381, 456, 473, 494 and 623 cm^{-1} owing to Si–O–Si of $[SiO_3]^{2-}$ in $SrSiO_3$ nano-crystals were found in glass-ceramics. Thus, the precipitation of lower phonon energy $SrSiO_3$ nano-crystals in the glass-ceramics and entrance of Eu^{2+}/Sm^{3+} into $SrSiO_3$ crystalline phase resulted in intense red, green and blue luminescence in comparison with glass.

Fig. 4 presents the PL spectra of the glass-ceramics with different Eu^{2+}/Sm^{3+} molar ratio, and their chromatic coordinates were calculated and plotted on the CIE-1931 chromaticity diagram, as shown in Fig. 9. As can be seen in Fig. 4, the emission intensity of Eu^{2+} and Sm^{3+} increased with increasing Sm_2O_3 concentration at the lower activator content. It reached the maximum intensity at the concentration of 0.04 mol Sm_2O_3, while decreased with a further increase of the Sm_2O_3 concentration. As for the emission intensity of Sm^{3+}, it can be explained by the concentration quenching [38]. A non-radiative energy transfer from one Sm^{3+} ions to another Sm^{3+} ions took place, which may occur through exchange interaction, radiation reabsorption and multipole–multipole interaction. The exchange interaction usually works for a forbidden transition and the typical critical distance is about 5 Å. Radiation reabsorption plays an important role when there is broad overlap between the excitation and emission spectra. A rough estimation of the critical distance of energy transfer (R_c) can be made using the relation given by Blasse [39] to calculate R_c between activator ions of the same kind when doped in a host lattice.

$$R_c \approx 2\left(\frac{3V}{4\pi x_c Z}\right)^{1/3} \quad (1)$$

where R_c corresponds to the critical separation between the nearest Sm^{3+} ions at the critical concentration, V is the volume of the unit cell, Z is the number of host cations in the unit cell, x_c is the critical concentration of activator ions. According to the crystal structure of the $SrSiO_3$ compound [32], V = 889.49 $Å^3$, Z = 12 and x_c = 0.08, R_c was reckoned to be 11.9 Å. Therefore it can be concluded that energy transfer between Sm^{3+} ions in $SrSiO_3$ nano-crystals should be electric multipole–multipole interaction.

Fluorescence decay analysis is very useful for understanding the energy transfer mechanism and quenching behavior of luminescence of Sm^{3+} and Eu^{2+} ions. The fluorescence decay curves corresponding to the emission line $^4G_{5/2} \rightarrow {}^6H_{7/2}$ at 600 nm with pulsed excitation at 365 nm were examined in terms of Sm^{3+} concentration, and they are shown in Fig. 5. The life time was estimated as 2.38 ms, 2.06 ms, 1.98 ms, 1.81 ms and 1.62 ms for GC1, GC2, GC3, GC4 and GC5 respectively. It can be seen from Fig. 5 that the concentration quenching is also made evident by the change from non-exponential to virtually single exponential decays of $^4G_{5/2}$ level with increasing Sm^{3+} concentration [40,41]. In order to verify the nature of the electric multipole–multipole interaction in this system, the non-exponential behavior of the decay curve has been fitted using Hirayama–Inokuti model. The resulting decay function has the form

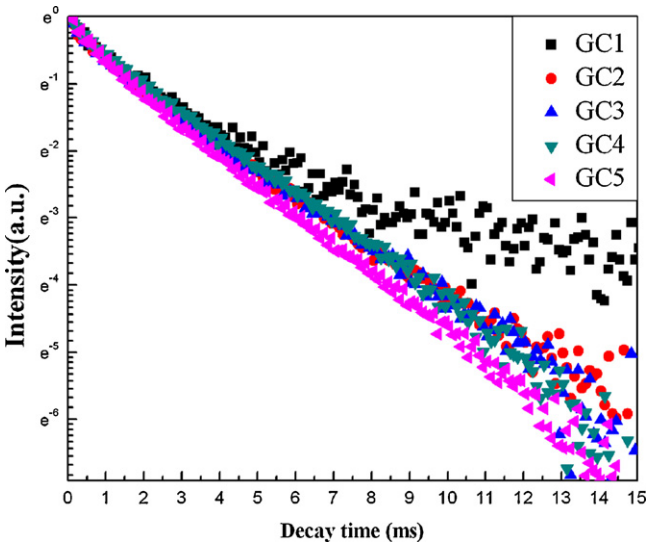

Fig. 5. The fluorescence decay curves of GC1, GC2, GC3, GC4 and GC5 corresponding to the emission line $^4G_{5/2} \rightarrow {}^6H_{7/2}$ at 600 nm with pulsed excitation at 365 nm. (For interpretation of the references to color in this figure legend, the reader is referred to the web version of the article.)

$$\frac{I(t)}{I_0} = \exp\left[-\frac{t}{\tau} - \alpha\left(\frac{t}{\tau}\right)^{3/S}\right] \quad (2)$$

where $I(t)$ is the emission intensity after pulsed excitation, I_0 is the intensity of the emission at t = 0, τ is the intrinsic lifetime of a single ion, α is a parameter containing the energy probability, and S is an indication of electric multipole character; S = 6, 8, 10 for dipole–dipole, dipole–quadrupole, quadrupole–quadrupole interactions, respectively [42]. The plot depicted in Fig. 6 of $\ln[-\ln(I(t)/I_0) - (t/\tau)]$ vs. $\ln(t/\tau)^3$ yields a straight line with a slope equal to $1/S$ [43]. The value of S estimated from the slope was found to be 5.63, 5.75, 6.11 and 6.46 for GC2, GC3, GC4 and GC5 respectively, which indicated the dipole–dipole interaction may be responsible for the energy transfer.

While the luminescence change of Eu^{2+} may be resulted by the energy transfer from Sm^{3+} to Eu^{2+}, which depended on the emission intensity of Sm^{3+}. So the emission intensity of Eu^{2+} exhibited similar fluctuations with that of Sm^{3+}. Fig. 7 shows the simplified energy level diagrams of the Sm^{3+} and Eu^{2+}, as well as a probably energy transfer mechanism. Generally, the lifetime of Sm^{3+} and Eu^{2+} are in ~ms and ~ns respectively [40,44]. When the $^4L_{27/2}$ level (365 nm) of Sm^{3+} is excited, the initial population firstly relaxes to the $^4K_{13/2}$, $^{(6,4)}P_{5/2}$, $^4G_{9/2}$, $^4G_{7/2}$ level, finally to the $^4G_{5/2}$ level. There is enough time and possibility for the emission from $^4K_{13/2}$, $^{(6,4)}P_{5/2}$, $^4G_{9/2}$, $^4G_{7/2}$ level to the ground state $^6H_{5/2}$ of Sm^{3+} being absorbed by the nearby Eu^{2+} ions. The fluorescence decay curve of Sm^{3+} single doped and Eu^{2+}/Sm^{3+} co-doped $SrSiO_3$ glass ceramics is shown in Fig. 8. The life time of Sm^{3+} decreased from 2.44 ms to 2.06 ms with co-doping Eu^{2+}, which indicated the existence of energy transfer from Sm^{3+} to Eu^{2+} too.

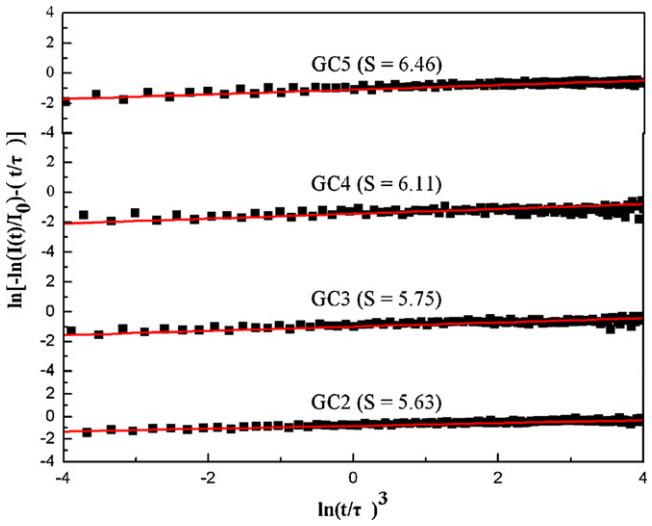

Fig. 6. Plots of experimental data $\ln[-\ln(I(t)/I_0)-(t/\tau)]$ vs. $\ln(t/\tau)^3$ of transition ($^4G_{5/2} \rightarrow {}^6H_{7/2}$) with the solid lines representing theoretical fits. (For interpretation of the references to color in this figure legend, the reader is referred to the web version of the article.)

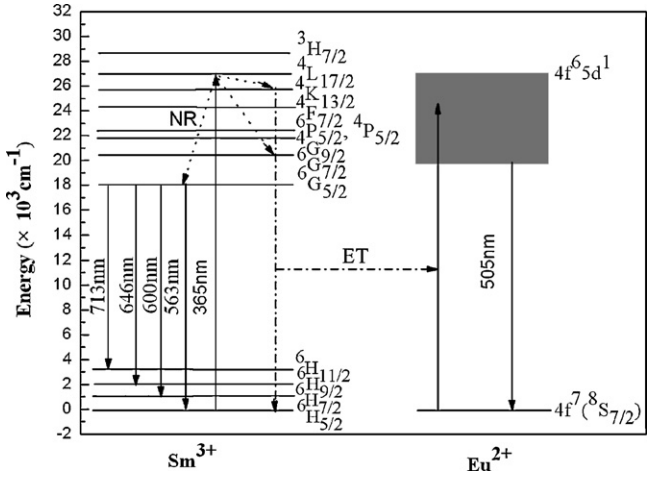

Fig. 7. Simplified energy level diagram and a probably energy transfer mechanism of Eu^{2+} and Sm^{3+} in $SrSiO_3$ glass ceramics.

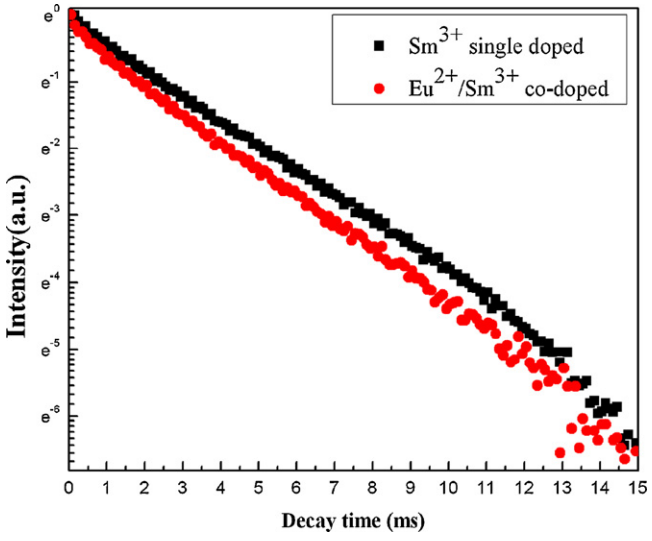

Fig. 8. The fluorescence decay curve of 0.08 mol Sm^{3+} single doped and 0.02 mol Eu^{2+}/0.08 mol Sm^{3+} co-doped $SrSiO_3$ glass ceramics. (For interpretation of the references to color in this figure legend, the reader is referred to the web version of the article.)

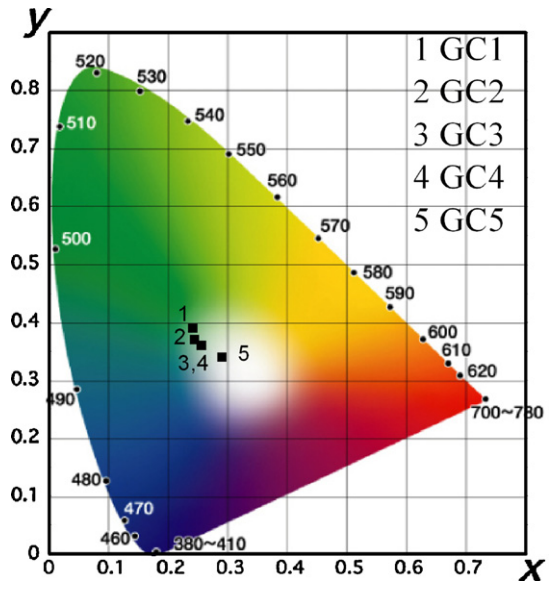

Fig. 9. CIE chromaticity coordinates of GC1, GC2, GC3, GC4 and GC5.

The CIE chromaticity coordinates of GC1, GC2, GC3, GC4 and GC5 were calculated according to their PL spectra and plotted on the CIE-1931 chromaticity diagram in Fig. 9. With increasing the concentration of Sm_2O_3, the chromaticity coordinate moved toward the optimal white light (0.33, 0.33), which could be attributed to the alteration of the PL spectra and the relative emission intensity of Eu^{2+} and Sm^{3+} ions. When the molar ratio of Eu^{2+}/Sm^{3+} was 1:10 (0.01 mol Eu_2O_3 and 0.1 mol Sm_2O_3), the Eu^{2+}/Sm^{3+} co-doped glass-ceramics got the best white light emission and the corresponding chromaticity coordinate was (0.29, 0.35).

4. Conclusions

Eu^{2+}/Sm^{3+} co-doped silicate glass was prepared by high temperature melting under reducing atmosphere and the Eu^{2+}/Sm^{3+} co-doped $SrSiO_3$ transparent glass-ceramics were obtained after heat-treatment. The broad PLE spectrum band from 300 to 420 nm showed an excellent overlap with the main emission region of an UV-LED chip. The emission of Eu^{2+} and Sm^{3+} in glass-ceramics was much stronger than that in glass, which could be attributed to the precipitated low phonon energy of $SrSiO_3$ nano-crystals in glass-ceramics. The UV-LED excitable glass-ceramics emitting white light were obtained by controlling the relative emission intensity of Eu^{2+}/Sm^{3+}. When the molar ratio of Eu^{2+}/Sm^{3+} is 1:10 (0.01 mol Eu_2O_3 and 0.1 mol Sm_2O_3), the Eu^{2+}/Sm^{3+} co-doped glass ceramics got the optimal white light emission and the corresponding chromaticity coordinate (0.29, 0.35) exactly fell into the white light area of the CIE-1931 chromaticity diagram. The results showed that the Eu^{2+}/Sm^{3+} co-doped $SrSiO_3$ transparent glass-ceramics phosphor can be applied as a potential matrix material for high power White LED pumped by UV-LED chip.

Acknowledgements

This work was financially supported by National Natural Science Foundation of China (Grant Nos. 51072190 and 11004177), Program for New Century Excellent Talents in University (NCET-07-0786) and Zhejiang Provincial Natural Science Foundation of China (Z4100030 and Y4080268).

References

[1] S. Nakamura, T. Mukai, M. Senoh, Appl. Phys. Lett. 64 (1994) 1687–1689.
[2] E.F. Schubert, J.K. Kim, Science 308 (2005) 1274.
[3] M.P. Saradhi, U.V. Varadaraju, Chem. Mater. 18 (2006) 5267–5272.
[4] T. Nishida, T. Ban, N. Kobayashi, Appl. Phys. Lett. 82 (2003) 3817–3819.
[5] Z.C. Wu, J. Liu, W.G. Hou, J. Xu, M.L. Gong, J. Alloys Compd. 495 (2010) 72–75.
[6] C.F. Guo, Y. Xu, X. Ding, M. Li, J. Yu, Z.Y. Ren, J.T. Bai, J. Alloys Compd. 509 (2011) L38–L41.
[7] H. He, X.F. Song, R.L. Fu, Z.W. Pan, X.R. Zhao, Z.H. Deng, Y.G. Cao, J. Alloys Compd. 493 (2010) 401–405.
[8] C.F. Guo, Y. Xu, F. Lv, X. Ding, J. Alloys Compd. 497 (2010) L21–L24.
[9] I.M. Nagpure, K.N. Shinde, S.J. Dhoble, A. Kumar, J. Alloys Compd. 481 (2009) 632–638.
[10] S.S. Yao, L.H. Xue, Y.W. Yan, J. Alloys Compd. (2010), doi:10.1016/j.jallcom.2010.10.076.
[11] A. Engel, M. Letz, T. Zachau, E. Pawlowski, K. Seneschal-Merz, T. Korb, D. Enseling, B. Hoppe, U. Peuchert, J.S. Hayden, Proc. SPIE 6486 (2007), 64860Y.1–64860Y.10.
[12] S. Tanabe, S. Fujita, A. Sakamoto, S. Yamamoto, Ceram. Trans. 173 (2006) 19–25.
[13] S. Nishiura, S. Tanabe, J. Ceram. Soc. Jpn. 116 (2008) 1096–1099.
[14] T. Nakanishi, S. Tanabe, Phys. Status Solidi (a) 206 (2009) 919–922.
[15] L.Y. Xiao, Q. Xiao, Y.L. Liu, P.F. Ai, Y.D. Li, H.J. Wang, J. Alloys Compd. 495 (2010) 72–75.
[16] S. Taruta, M. Matsuki, H. Nishikiori, T. Yamakami, T. Yamaguchi, K. Kitajima, Ceram. Int. 36 (2010) 1303–1309.
[17] Q. Luo, X.S. Qiao, X.P. Fan, X.H. Zhang, J. Non-Cryst. Solids 356 (2010) 2875–2879.
[18] D.Q. Chen, Y.L. Yu, P. Huang, H. Lin, Z.F. Shan, Y.S. Wang, Acta Mater. 58 (2010) 3035–3041.
[19] A. Diaz, D.A. Keszler, Mater. Res. Bull. 31 (1996) 147–151.
[20] S.H.M. Poort, W. Janssen, G. Blasse, J. Alloys Compd. 260 (1997) 93–97.
[21] J.S. Kim, P.E. Jeon, Y.H. Park, J.C. Choi, H.L. Park, Appl. Phys. Lett. 85 (2004) 3696–3698.
[22] D.H. Gahane, N.S. Kokode, P.L. Muthal, S.M. Dhopte, S.V. Moharil, J. Alloys Compd. 484 (2009) 660–664.
[23] L.J. Nugent, R.D. Baybarz, J.L. Burnett, J.L. Ryan, J. Phys. Chem. 73 (1969) 1177–1178.
[24] S.H.M. Poort, H.M. Reijnhoudt, H.O.T. van der Kuip, G. Blasse, J. Alloys Compd. 241 (1996) 75–81.
[25] K. Machida, G. Adachi, J. Shiokawa, M. Shimada, M. Koizumi, K. Suito, A. Onodera, Inorg. Chem. 21 (1981) 1512–1519.
[26] I. Nobuya, U. Norimasa, D. Kenji, Trans. JWRI 11 (1982) 55–59.
[27] C. Karlsson, E. Zanghellini, J. Swenson, B. Roling, D.T. Bowron, L. Börjesson, Phys. Rev. B 72 (2005) 064206.
[28] D.J. durben, G.H. Wolf, Am. Mineral 77 (1992) 890–893.
[29] K. Annapurna, R.N. Dwivedi, P. Kundu, S. Buddhudu, Mater. Res. Bull. 38 (2003) 429–436.
[30] G. Lakshminarayana, R. Yang, M.F. Mao, J.R. Qiu, I.V. Kityk, J. Non-Cryst. Solids 355 (2009) 2668–2673.
[31] J.S. Kim, P.E. Jeon, J.C. Choi, H.L. Park, Solid State Commun. 133 (2005) 187–190.
[32] K.I. Machida, G.Y. Adachi, J. Shiokawa, M. Shimada, M. Koizumi, Acta Crystallogr. B 38 (1982) 386–389.
[33] M. Yang, S.Y. Zhang, J. Phys. Chem. Sol. 64 (2003) 213–221.
[34] S.H.M. Poort, W.P. Blokpoel, G. Blasse, Chem. Mater. 7 (1995) 1547–1551.
[35] M.Y. Peng, Z.W. Pei, G.Y. Hong, Q. Su, J. Mater. Chem. 13 (2003) 1202–1205.
[36] Q. Luo, X.P. Fan, X.S. Qiao, H. Yang, M.Q. Wang, J. Am. Ceram. Soc. 92 (2009) 942–944.
[37] M. Rozanski, K. Wisniewski, J. Szatkowski, C. Koepke, M. Środa, Opt. Mater. 31 (2009) 548–553.
[38] P.L. Li, Z.J. Wang, Z.P. Yang, Q.L. Guo, X. Li, Mater. Lett. 63 (2009) 751–753.
[39] G. Blasse, Philips Res. Rep. 24 (1969) 131–144.
[40] T. Suhasini, J.S. Kumar, T. Sasikala, K. Jang, H.S. Lee, M. Jayasimhadri, J.H. Jeong, S.S. Yi, L.R. Moorthy, Opt. Mater. 31 (2009) 1167–1172.
[41] X.M. Zhang, H.J. Seo, J. Alloys Compd. 503 (2010) L14–L17.
[42] M. Inokuti, F. Hirayama, J. Chem. Phys. 43 (1965) 1978–1989.
[43] K.S. Sohn, Y.Y. Choi, H.D. Park, J. Electrochem. Soc. 147 (2000) 1988–1992.
[44] W.J. Yang, L.Y. Luo, T.M. Chen, N.S. Wang, Chem. Mater. 17 (2005) 3883–4388.